INFLUENCE OF NUCLEAR LEVEL DENSITY AND GAMMA STRENGTH FUNCTION ON NEUTRON CAPTURE REACTION RATE

Cosmina Viorela Nedelcu[1,2], Yi Xu[1], Dimiter L. Balabanski[1,2]

Neutron-induced reactions are an essential part of the nucleosynthesis process. In the present study, neutron capture cross-sections and reaction rates are systematically studied considering the nuclear structure obtained from microscopic and phenomenological models. In particular, the nuclear level density (NLD) derived from the microscopic Hartree-Fock-Bogoliuboiv plus combinatorial method and the phenomenological Constant Temperature model, and the γ-ray strength function (γSF) determined by the semi-microscopic Gogny D1M interaction plus Quasi Random Phase Approximation and the global empirical Standard Modified Lorentzian are taken into account in the calculation, and the results are compared to the available experimental Maxwellian-averaged cross-sections. It is demonstrated that the experimental data are well reproduced by the nuclear structure models considered here, and the predictive power of these nuclear ingredients is very close. Furthermore, a sensitivity study of neutron capture reaction to the available nuclear ingredients for unstable nuclei, e.g. for ^{89}Zr, is performed, which indicates that the NLD and γSF can considerably influence the cross-section and reaction rate. Therefore, we investigate the applicability of the NLD and γSF obtained from the analysis of stable nuclei to the calculations of all eight unstable nuclei of which the NLDs are experimentally determined so far. A good agreement of the astrophysical reaction rates predicted by the aforementioned nuclear structure ingredients is found.

Keywords: nuclear level density, gamma strength function, neutron capture cross-section, astrophysical reaction rate

[1] Extreme Light Infrastructure - Nuclear Physics (ELI-NP), Horia Hulubei National Institute for R&D in Physics and Nuclear Engineering (IFIN-HH), 077125 Bucharest - Magurele, Romania

[2] Doctoral School in Engineering and Applications of Lasers and Accelerators, National University of Science R&D Technology POLITEHNICA Bucharest, 060042 Bucharest, Romania

* corresponding author: e-mail: cosmina.nedelcu@eli-np.ro

1. Introduction

The creation of elements heavier than iron remains a significant challenge within stellar nucleosynthesis. The bulk of these isotopes are assumed to be formed by three mechanisms: the rapid neutron capture process (r-process), the slow neutron capture process (s-process), and the proton capture process (p-process). The s-process takes place over a lengthy period ($\sim 10^3$ years between captures), allowing unstable nuclei to decay before stabilizing through neutron capture. In this way, stable isotopes along the β-stability valley are created. The s-process is characterized by a low neutron density (10^6 - 10^{10} cm^{-3}) and occurs in massive stars, particularly in the asymptotic giant branch stars. Since it proceeds extremely slowly, β-decay occurs before capturing a neutron, creating stable isotopes along the stability valley [1]. On the contrary, the r-process is a fast process, lasting for a few seconds or less. It is associated with rapid neutron captures (100 captures/ second) by one or more heavy seed nuclei, often beginning with nuclei centered on the iron peak. As these captures are so fast, nuclei do not have time to decay before another neutron is captured. The series repeats itself until a balance is reached between further neutron captures and reverse photodisintegration facilitated by the energetic photon environment, extending towards the neutron drip line. The dominance of the r-process occurs in environments characterized by a high flux of free neutrons (greater than 10^{20} cm^{-3}) and temperatures exceeding 6 to 8 $\times$ 10^9 K. The exact location where the r-process occurs remains elusive due to its specific requirements, although the merging of two neutron stars stands out as a likely scenario. Therefore, the r-process involves many unstable nuclei with properties that cannot be acquired through present-day experiments [2].

Determining the cross-section and reaction rate of (n,γ) within these processes poses a significant challenge, particularly for the r-process, where experimental data is limited. Until now, no method exists for direct determination of the neutron capture cross-section of short-lived nuclei because of their short lifetime, as well as the fact that neutrons do not have charge, making them unsuitable for accelerator-based experiments. Direct measurements of (n,γ) cross-sections are feasible for stable nuclei or nuclei with long half-lives. Thus, the determination of (n,γ) cross-sections for short-lived nuclei far from stability is challenging and relies on theoretical approaches [3].

Several indirect methods have been proposed [4] for estimating the neutron capture cross-section, including the γ strength function (γSF) method [5], surrogate reaction methodology [6], and the Oslo method [7]. Another technique which involves γ-ray measurements was introduced not long ago, namely the β-Oslo technique [8, 9, 3, 10, 11, 12, 13, 14]. It is a mix of the traditional Oslo analysis, β-decay, and total absorption spectroscopy. Its advantage lies in its usability with extremely low beam intensities, even as low as one particle

per second or less. Thus, it enables further exploration from the β-stability valley than reaction-based methods [12]. Both Oslo and β-Oslo approaches simultaneously extract fundamental nuclear properties, such as γSF and nuclear level density (NLD), from experimental data while constraining the neutron capture cross-section within the statistical reaction model [8]. These techniques differ in the population mechanism of decay, *e.g.*, the β-Oslo method uses β-decay to populate the highly excited states in the daughter nucleus, which subsequently undergo de-excitation via γ-ray emission. In contrast, the Oslo method relies on light-charged particle reactions [11].

This paper is organized as follows: the statistical Hauser-Feshbach (HF) model and the associated nuclear ingredients for neutron capture reaction are described in Sections 2 and 3, respectively. Studies of the neutron capture cross-sections and reaction rates involving the NLD and γSF for both stable and unstable nuclei are presented in Section 4. Conclusions are summarized in Section 5.

2. **Statistical Hauser-Feshbach model for neutron capture**

The radiative neutron capture is described by the statistical Hauser-Feshbach (HF) formalism. This approach is based on the assumption that the capture process relies on the intermediary creation of a compound nucleus (CN) in thermodynamic equilibrium. The CN is produced with high excitation energy, allowing the interaction of the incoming particle with the target to excite numerous states. Additionally, the incident energy is dispersed uniformly among all nucleons, leading to complete equilibrium before the decay begins. Therefore, the memory of its formation is lost. In simpler terms, the compound system (CS) formation and its subsequent decay occur independently. Within the HF model, the existence of the CN is justified due to its NLD at the projectile incident energy which is large enough to allow an average statistical continuum superposition of the available resonances [15].

Considering the capture reaction *A(n,γ)B*, the binary reaction cross-section can be written as

$$\sigma^{CNC}(E) = \sum_{x=0}^{B} \sigma^{CNC}_{A+n\rightarrow B^x+\gamma} \tag{1}$$

The summation $\sum_{x=0}^{B}$, where the energy-level scheme is represented by the x-th excited state ($x = 0$ is the ground state), covers all the ground and all possible excited states of the residual nucleus B. Each state is characterized by a spin I^x_B, a parity π^x_B, and an excitation energy E^x_B for the residual nucleus

B. Furthermore, the cross-section $\sigma^{CNC}_{A+n\rightarrow B^x+\gamma}$(E) can be expressed as

$$\begin{aligned}\sigma^{CNC}_{A+n\rightarrow B^x+\gamma} = \frac{\pi}{k^2}\sum_{J=mod(I_A+I_n,1)}^{l_{max}+I_A+I_n}\sum_{\Pi=-1}^{1}\frac{2J+1}{(2I_A+1)(2I_n+1)}\\ \times\sum_{J_p=|J-J_A|}^{J+I_A}\sum_{l_i=|J_n-I_n|}^{J_n+I_n}\sum_{\lambda=|J-I^x_B|}^{J+I^x_B}\sum_{l_f=|\lambda-I_\gamma}^{\lambda+I_\gamma}\delta^{\pi}_{C_n}\delta^{\pi}_{C_\gamma}\\ \times\frac{\langle T^J_{C_n,l_i,J_n}(E)\rangle\langle T^J_{C_\gamma,l_f,\lambda}(E_\gamma)}{\sum_{Clj}\delta^{\pi}_{C}\langle T^J_{C,l,j}(E_C)\rangle}W^J_{C_n l_i J_n C_\gamma l_f \lambda}\end{aligned} \tag{2}$$

where k is the wave number of the relative motion, E is the incident energy of the neutron, and E_γ is the energy of the emitted photon. In this equation, l_{max} is the maximum value of the relative orbital momentum l_i of $A + n$, l_f is the relative orbital momentum of the residual nucleus B and the photon, I_n, J_n, and π_n are the spin, total angular momentum, and parity of the neutron, respectively; I_γ and π_γ are the spin and parity of the photon, respectively; λ is the multipolarity of the photon (total angular momentum of photon) coupled by I_γ and l_f; J and π are the total angular momentum and parity of the compound nucleus; C_n is the channel label of the initial system *(n + A)* designated by C_n = *(n,* I_n*,* E*,* $E_n = 0$*,* I_A*,* π_A*)*; C_γ is the channel label of the final system ($\gamma + B^x$) designated by $C_\gamma = (\gamma,\ I_\gamma,\ E_\gamma\ ,\ E^x_B,\ I^x_B,\ \pi^x_B)$; concerning the δ functions, they enforce the conformity with the parity conservation rules, $\delta^{\pi}_{C_\gamma} = 1$ if $\pi_A\pi_n(-1)\ l_i = \Pi$ and 0 otherwise; $\delta^{\pi}_{C_\gamma} = 1$ if $\pi^x_B\pi_\gamma(-1)\ l_f = \Pi$ and 0 otherwise; T is the transmission coefficient that represents the probability of a CN to be created; $W^J_{C_n l_i J_n C_\gamma l_f \lambda}$ is the width fluctuation correction factor which accounts for channel correlations and $\sum_{Clj}\delta^{\pi}_{C}\langle T^J_{C,l,j}(E_C)\rangle$ is the sum of the transmission coefficient for all possible decay channels C. Each transmission coefficient T is calculated for all levels with known parity, spin, and energy. If the excitation energy corresponds to a state in the continuum, an effective transmission coefficient for an excitation-energy bin of width ΔE is defined by the integral

$$\langle T^J_{C,l,j}(E_C)\rangle = \int_{E_x-\Delta E/2}^{E_x+\Delta E/2}\rho(E,J,\pi)T^J_{Clj}(E_C)dE \tag{3}$$

over the nuclear level density $\rho(E, J, \pi)$ [16].

Furthermore, the neutron-induced reaction rate can be written as

$$N_A\langle\sigma v\rangle = N_A\left(\frac{8}{m\pi}\right)^{1/2}\cdot\frac{1}{(k_BT)^{3/2}}\int_0^\infty E\cdot\sigma(E)\cdot e^{-E/k_BT}dE \tag{4}$$

where N_A is Avogadro's number, m is the reduced mass, k_B is the Boltzmann constant, E is the center-of-mass energy, and ν is the relative velocity between target and projectile [17].

3. Nuclear ingredients for neutron-capture calculation

The statistical HF theory facilitates the calculation of the cross-section determined by three essential components - the nuclear level-scheme, the optical model potential (OMP), and the γSF. The sensitivity of the neutron capture cross-section to OMP has been well addressed [18], and will not be considered here. In the present study, we focus on NLD and γSF. The NLD defines the number of excited states of a CN in a given energy, crucial for the statistical nuclear reaction calculation, and the γSF represents the nuclear response to the emission or absorption of a γ-ray with a specific energy. Together, they establish the probability of nuclei to decay via photon emission after catching a neutron [10].

In particular, at energies of astrophysical interest, the CN capture is the predominant reaction mechanism for heavy- and medium-mass nuclei lying within the β-stability valley. The CS presents a discrete structure of excited levels at low excitation energies. Increasing this energy, they become nearly uniform, making them indistinguishable. To solve this issue, excited levels are estimated by the theoretical NLD [15]. On the other hand, extrapolating data far from the experimentally known region is necessary for nuclear astrophysics, and reliable and accurate nuclear ingredients, especially the NLD, should be considered. Within the HF formalism, the NLD used for the calculation of the radiative cross-section is defined by the following formula

$$\rho_{tot}(E_x) = \sum_{J} \sum_{\pi} \rho(E_x, J, \pi) \tag{5}$$

with excitation energy E_x, spin J and parity π. $\rho(E_x, J, \pi)$ is the NLD that corresponds to the number of levels per MeV of a specific parity and spin and $\rho_{tot}(E_x)$ represents the total NLD obtained by summing over spin and parity the $\rho(E_x, J, \pi)$ [19].

Another critical ingredient in the accurate calculation of neutron capture cross-section is the γSF. It is rooted in statistical physics and used in a nuclear system with sufficiently high excited states and high NLD to treat the γ-excitation and decay statistically. It quantifies the average probability of γ-ray absorption or emission at a given energy in this context. From eq.(2), the link between the transmission coefficient and γSF is given by [19]

$$T(E_\gamma) = 2\pi f_{E1}(E_\gamma) E_\gamma \tag{6}$$

where $f_{E1}(E_\gamma)$ is the electric-dipole *E1* photon strength function.

4. Result and discussion

4.1. Verification of nuclear ingredients for stable nuclei

In Ref.[4], it has been demonstrated that the microscopic NLD derived from the Hartree-Fock-Bogoliuboiv plus combinatorial (HFB + comb.) method and the phenomenological Constant Temperature (CT) NLD provide the most accurate description of the experimental data for stable nuclei, based on a comprehensive analysis of the available data of NLD measured by the Oslo method. Despite the variations in spin, parity, and energy dependencies within the descriptions of the NLD, both models have proven capable of closely replicating the experimental data. However, determining further a definitive preference among these models remains challenging based on this comprehensive evaluation.

On the other hand, in Ref.[20] was suggested that the best description of the experimental data for stable nuclei is given by the global empirical Standard Modified Lorentzian (SMLO) or the semi-microscopic Gogny D1M interaction plus Quasi Random Phase Approximation (D1M HFB QRPA) γSF models. They characterize both magnetic and electric dipole γSFs. Additionally, the global SMLO models have been validated against measured average radiative widths and Maxwellian-averaged cross-sections (MACS), suggesting their reliability for the extrapolation to experimental unknown nuclei and as valuable references when experimental data are limited. Nevertheless, the global comparisons have revealed certain limitations inherent in these models, suggesting that moving beyond QRPA represents the future direction. The QRPA approach interprets the nuclear excitation as a collective superposition of two quasi-particle states built on top of the HFB ground state, which makes it a reliable instrument for studying the photon strength function in both closed and open-shell nuclei. In practical calculations, the HFB plus QRPA technique investigates the nuclear structure characteristics of both ground state and collective excitation for nuclei ranging from the β-stability valley to the drip line in a self-consistent manner [21].

Here, we verify the results presented in Refs.[4] and [20] through a compressive examination of neutron capture cross-section for stable nuclei, using the two suggested NLD and γSF models. Figs. 1 and 2 present the ratio of the neutron capture cross-sections at $kT = 30$ KeV obtained in our calculation and the measured data analyzed in Ref.[22] or taken from the Kadonis database [23] *vs* the mass number A (from 0 to 220) for light up to heavy stable nuclei. Ref.[22] covers the measured data of stable nuclei up to the year 2000, whereas the Kadonis database provides an updated compilation extending up to the year 2020. To ensure comprehensive coverage, this analysis incorporates all stable nuclei studied and documented in the literature. The

input combines the two sets of NLD and γSF suggested in Refs.[4] and [20], including the phenomenological CT and the microscopic HFB + comb. method and the phenomenological SMLO and the semi-microscopic D1M HFB QRPA. The standard deviation f_{rms} consistently takes values of approximately one across all cases, indicating a near-constant level of precision. This uniformity suggests that these four models accurately replicate the experimental data for stable nuclei, demonstrating equivalent predictive power.

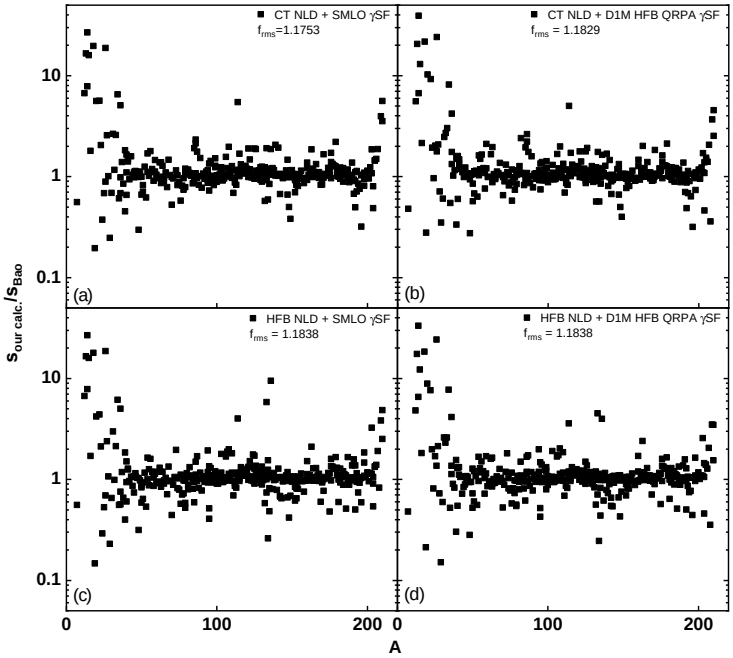

FIGURE 1. Ratio of the neutron capture cross-sections at $kT = 30$ KeV obtained in our calculation to the measured data analyzed by Ref.[22] *vs* the mass number A for stable nuclei. Different combinations of two NLD models and two sets of γSF are used, such as graph (a) contains the phenomenological CT NLD and phenomenological SMLO γSF, graph (b) shows the phenomenological CT NLD and the semi-microscopic D1M HFB QRPA γSF, graph (c) shows the microscopic HFB + comb. method for NLD and the phenomenological SMLO for γSF, and graph (d) presents the microscopic HFB + comb. method NLD and the semi-microscopic D1M HFB QRPA γSF.

4.2. Influence of neutron capture reactions to NLD and γSF for unstable nuclei

In the above section, we have verified the capability of the NLD and γSF sets outlined in Refs.[4] and [20] to replicate the experimental data for stable nuclei faithfully. We further investigate the sensitivities of neutron capture reactions to the nuclear structure, namely the available NLD and

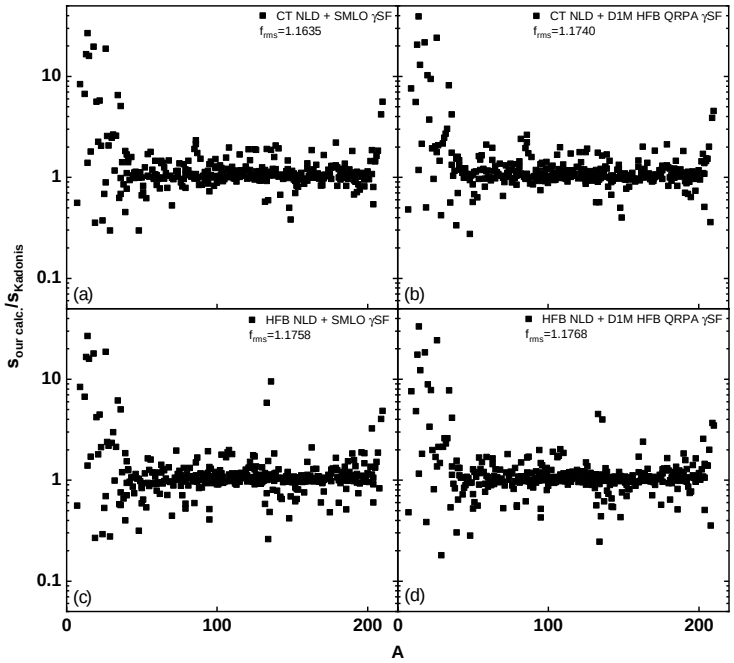

FIGURE 2. Ratio of the neutron capture cross-sections at $kT = 30$ Kev obtained in our calculation and the measured data taken from the Kadonis database *vs* the mass number A for stable nuclei. Different combinations of two NLD models and two sets of γSF are used, such as graph (a) contains the phenomenological CT NLD and phenomenological SMLO γSF, graph (b) phenomenological CT NLD and the semi-microscopic D1M HFB QRPA γSF, graph (c) microscopic HFB + comb. method for NLD and the phenomenological SMLO for γSF, and graph (d) microscopic HFB + comb. method NLD and the semi-microscopic D1M HFB QRPA γSF.

γSF, for the unstable nuclei that have not been checked before. In particular, we calculate the neutron capture cross-sections and reaction rates for the unstable nucleus ^{89}Zr using six sets of NLD models, such as the Constant Temperature (CT), the back-shifted Fermi gas (BFM), the generalized superfluid model (GSM), the Skyrme-Hartree-Fock plus statistical (HF + stat.), the Skyrme-Hartree-Fock-Bogoliubov plus combinatorial method (HFB + comb.), the temperature-dependent Gogny-Hartree-Fock-Bogoliubov plus combinatorial method (THFB + comb.) and eight sets of γSF, like the Kopecky-Uhl generalized Lorentzian (Gen.LO), the Brink-Axel Lorentzian (BALO), the Skyrme-Hartree-Fock-Bogoliubov (HFB), the Goriely's hybrid model (Hybr.), the Goriely's temperature-dependent HFB (THFB), the Temperature-dependent Relativistic Mean Field (TRMF), the Gogny Hartree-Fock-Bogoliubov (D1M HFB + QRPA), the Standard Modified Lorentzian (SMLO).

Fig. 3 illustrates the impact of these six available NLD models on the calculations of cross-sections and reaction rates. Here, graph (a) presents

the NLD models and their differences while maintaining a constant reaction energy of 1 MeV, with the NLDs normalized to the one obtained from the phenomenological CT model. Graphs (b) and (c) show the corresponding calculated neutron capture cross-sections and reaction rates normalized to the result obtained from the CT model. The data of the first four models (BFM, GSM, HF + stat., and HFB + comb.) vary slightly from each other, resulting in a small difference between them. In contrast, the THFB + comb. method consistently deviates from the other models, showing a difference of a factor of 10. The fluctuations observed in the data highlight the sensitivity of (n,γ) cross-section and reaction rate to NLD, which makes it a key variable in calculating the neutron capture parameters of astrophysical interest.

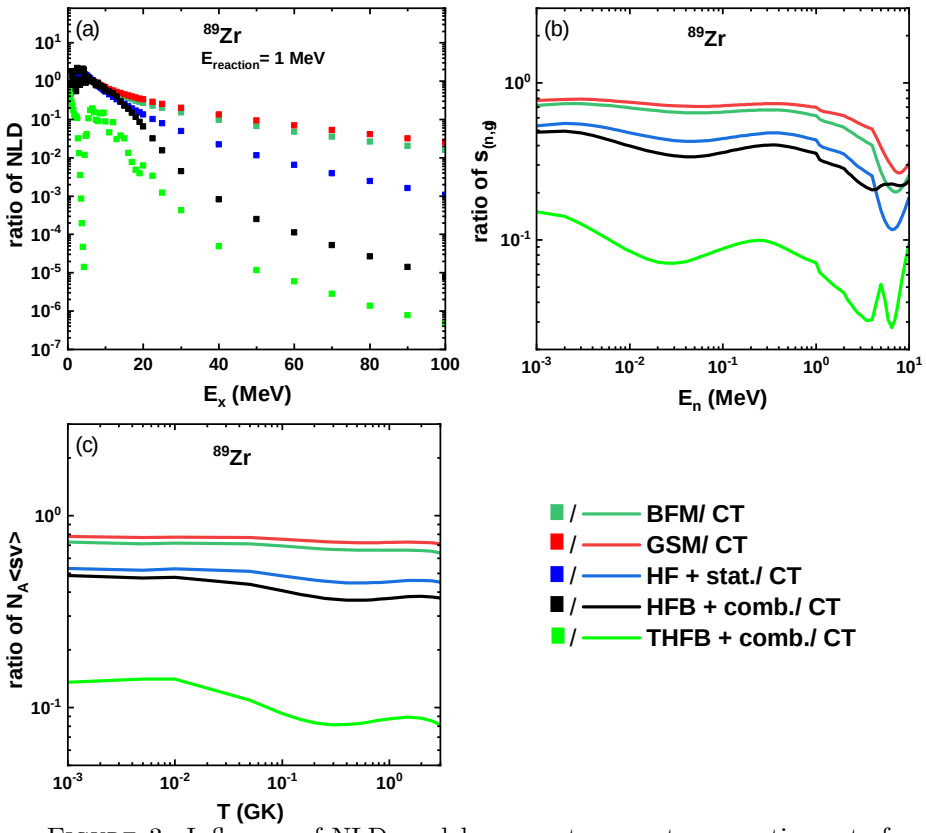

FIGURE 3. Influence of NLD models on neutron capture reaction rate for the unstable isotope ^{89}Zr. Graph (a) shows the available NLDs normalized to the one obtained from the phenomenological CT model when the reaction energy is 1 MeV. Graphs (b) and (c) present the corresponding calculated neutron capture cross-sections and reaction rates normalized to the CT model.

Fig. 4 shows the influence of various γSF on the calculation for ^{89}Zr. In graph (a), the γSFs are illustrated and normalized to the phenomenological SMLO, where all the ratios are close to one, indicating minor discrepancies

between the γSF models. Subsequently, graphs (b) and (c) present the corresponding radiative cross-sections and reaction rates normalized to the SMLO γSF. All these ratios are close to one in these cases too, except the TRMF model (orange line) which deviates by a factor of two from the others.

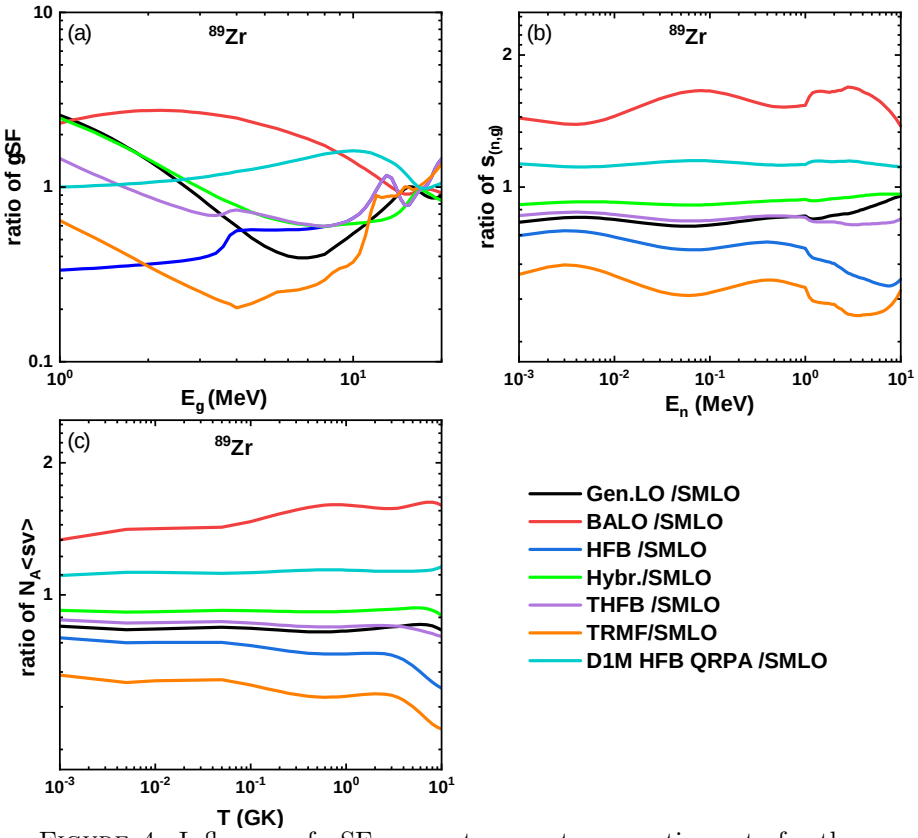

FIGURE 4. Influence of γSF on neutron-capture reaction rate for the unstable isotope ^{89}Zr. Graph (a) shows the available γSFs normalized to the phenomenological SMLO γSF. Graphs (b) and (c) present the corresponding neutron capture cross-sections and reaction rates normalized to the SMLO γSF.

The results presented in Figs. 3 and 4 show the substantial influence of both NLD and γSF on the calculations of neutron capture cross-sections and reaction rates. Notably, NLD appears as a very significant factor influencing the result.

4.3. Verification of nuclear ingredients for unstable nuclei with measured NLD

For the verification of the applicability of the nuclear properties suggested by Refs.[4] and [20] to unstable nuclei, we compare the theoretical NLD with the NLD measured with the β-Oslo method and radioactive ion beams

for eight unstable nuclei and extend the calculations of cross-sections and astrophysical reaction rates with the same nuclear ingredients used for the verification of stable nuclei, namely the CT and HFB + comb. method for NLD and D1M QRPA and SMLO for γSF. The experimental NLDs for all eight unstable nuclei that have been measured so far are considered in the present study.

Fig. 5 compares the experimental NLD (blue squares) and the two NLD models suggested in Ref.[4], the phenomenological CT (orange line) and the microscopic HFB + comb. method (black line) as a function of the excitation energy (0 - 10 MeV) for eight unstable nuclei (^{51}Ti [8], ^{67}Ni [9], ^{69}Ni [3], ^{70}Ni [10], ^{74}Zn [11], ^{76}Ge [12], ^{88}Kr [13], and ^{127}Sb [14]). The comparison suggests that both models can fairly reproduce the experimental data, however, the microscopic HFB prediction provides a relatively better description, especially for ^{127}Sb and ^{74}Zn. It is found that the fluctuation of the experimental data at lower energies is notable, *e.g.*, for ^{76}Ge, which is not well reproduced by the theoretical predictions.

Consequently, Figs. 6 and 7 present the corresponding (n,γ) cross-sections and astrophysical reaction rates for the eight unstable nuclei analyzed above. All the results are normalized to the one obtained from the microscopic HFB + comb. NLD plus the semi-microscopic D1M HFB QRPA γSF, as follows: CT + D1M HFB QRPA (red line), HFB + SMLO (black line), and CT + SMLO (blue line). The dashed green line is used to guide the eyes. For the neutron capture cross-section, a good agreement among these results is generally found, while at neutron energies above 1 MeV, the discrepancy reaches a factor of eight for ^{67}Ni. Therefore, our future work is expected to identify the NLD energy range critical to the cross-section calculations in such neutron-induced energies. For the reaction rate, overall a good agreement is achieved in all cases, indicated by the ratios less than 2 below $T = 5$ GK. This means that the two NLDs and two γSFs obtained from the analysis of stable nuclei provide quite similar reaction rates for these unstable nuclei.

5. **Conclusions**

The present study examines the sensitivity of neutron capture reactions to nuclear structure properties, such as NLD and γSF. The neutron capture cross-sections and astrophysical reaction rates are investigated using the nuclear ingredients derived from both phenomenological and microscopic models. Specifically, the radiative cross-sections obtained from the suggested models (the microscopic HFB + comb. method and phenomenological CT NLD models and the global empirical SMLO and the semi-microscopic D1M QRPA γSFs) are compared to the measured data of stable nuclei analyzed in Ref.[22] or taken from the Kadonis database (experimental MACS) at $kT = 30$ KeV. In this way, our analysis contains most available experimental neutron

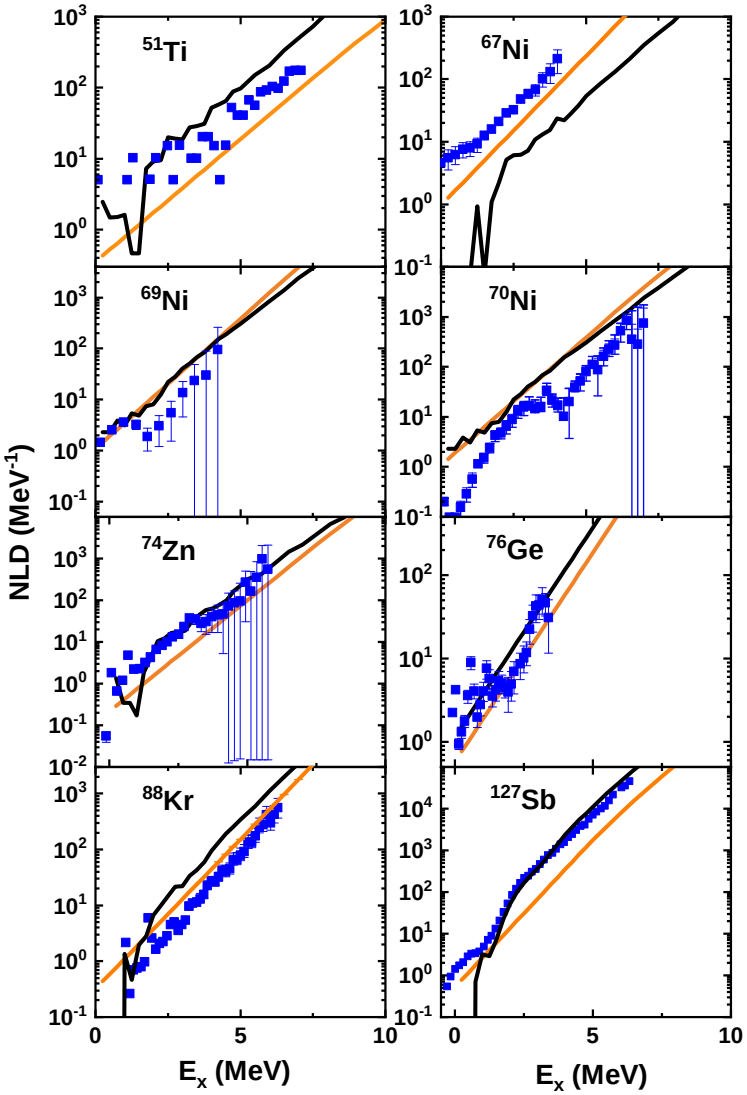

FIGURE 5. Comparison of theoretical NLD models (phenomenological CT in orange and microscopic HFB + comb. method in black) and the NLD measured by the β-Oslo and radioactive beam (blue squares) for eight unstable nuclei (^{51}Ti [8], ^{67}Ni [9], ^{69}Ni [3], ^{70}Ni [10], ^{74}Zn [11], ^{76}Ge [12], ^{88}Kr [13], and ^{127}Sb [14]).

capture cross-section of stable nuclei covering a wide range of nuclear mass from A = 20 to A = 220. It is found that these four models accurately reproduce the experimental data of stable nuclei, showing a standard deviation of approximately $f_{rms} = 1$ for each case.

Furthermore, the impact of NLD and γSF on neutron capture reactions is studied for unstable nuclei. In particular, we calculate the (n,γ) cross-sections and reaction rates for the unstable nucleus ^{89}Zr, considering the

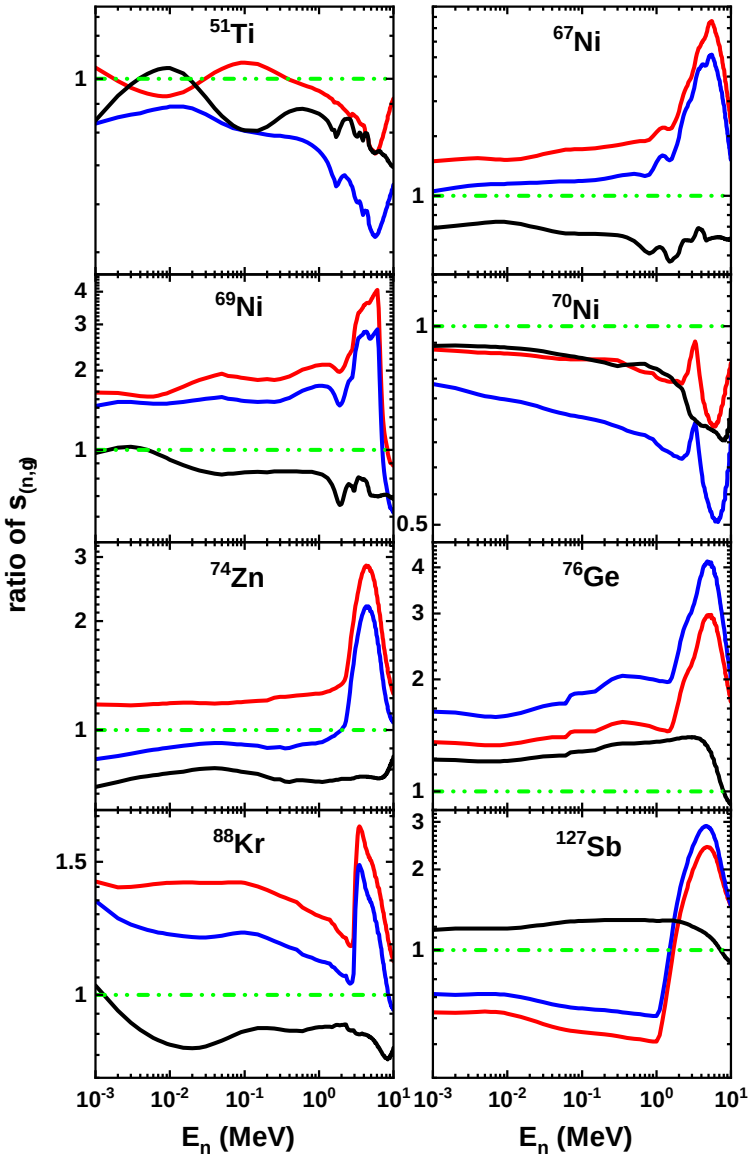

FIGURE 6. Ratio of the radiative neutron capture cross-sections of unstable nuclei analyzed in Fig. 5. Different combinations of two NLD models (phenomenological CT and microscopic HFB + comb. method) and two sets of γSF (phenomenological SMLO and the semi-microscopic D1M HFB QRPA) are used. All results are normalized to the one obtained from the microscopic HFB NLD model plus D1M HFB QRPA γSF, as follows: CT + D1M HFB QRPA (red line), HFB + SMLO (black line), and CT + SMLO (blue line). The dashed green line is used to guide the eyes.

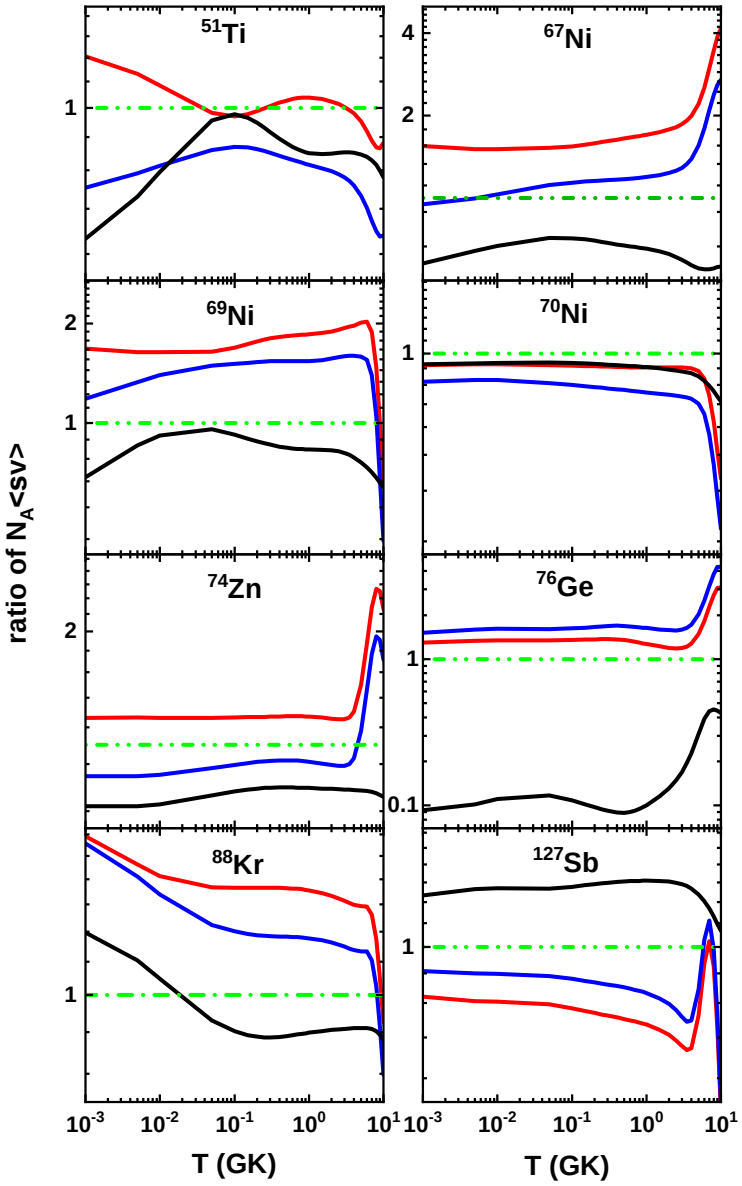

FIGURE 7. Ratio of astrophysical reaction rates of the unstable nuclei analyzed in Fig. 5. Different combinations of two NLD models (phenomenological CT and microscopic HFB + comb. method) and two sets of γSF (phenomenological SMLO and the semi-microscopic D1M HFB QRPA) are used. All results are normalized to the one obtained from the microscopic HFB NLD model plus D1M HFB QRPA γSF, as follows: CT + D1M HFB QRPA (red line), HFB + SMLO (black line), and CT + SMLO (blue line). The dashed green line is used to guide the eyes.

available sets of NLD and γSF. As these models significantly influence the calculation, the investigation was extended by including eight unstable nuclei measured with the β-OSlo technique in radioactive ion beam experiments. This study incorporates all unstable nuclei for which relevant experimental NLDs are available in the literature. Specifically, we compare the experimental NLD and the two suggested NLDs. Both models have proven capable of reproducing the experimental data, but the HFB predictions give a better description, especially for ^{74}Zn and ^{127}Sb. At low energies, fluctuations of experimental data are observed, especially for ^{76}Ge. The corresponding (n,γ) cross-sections and astrophysical reaction rates are calculated, with all the results normalized to the one obtained from the microscopic HFB + comb. NLD and the semi-microscopic D1M HFB QRPA γSF. A good agreement among all the results is generally found for the cross-sections. At neutron energies above 1 MeV, the discrepancy reaches a factor of eight for ^{67}Ni. Therefore, in the future, we will investigate the most sensitive energy range of NLD to cross-section in such neutron-induced energies. Overall, a good agreement among all the results is also found for the reaction rate, indicated by the ratios less than two below T = 5 GK. All these indicate that the suggested NLD models (the microscopic HFB + comb. method and the phenomenological CT) and the two sets of γSFs (the semi-microscopic D1M HFB QRPA and the global empirical SMLO) obtained from the analysis of stable nuclei provide quite similar reaction rates for the studied unstable nuclei.

Acknowledgments

This work is supported by the Romanian Ministry of Research, Innovation and Digitalization under Contract PN 23.21.01.06, the ELIRO projects with the Contracts ELI-RO_RDI_2024_007 and ELI-RO_RDI_2024_008(AMAP), the grant of the Romanian Ministry of Research, Innovation and Digitization, CNCS - UEFISCDI, with the project number PN-III-P4-PCE-2021-1014, PN-III-P4-PCE-2021-0595, and PN-III-P1-1.1-TE2021-1464 within PNCDI III, the IAEA CRP on "Updating and Improving Nuclear Level Densities for Applications" (F41034), and the Institute of Atomic Physics Romania, Project ELIRO/DFG/2023_001 ARNPhot.

REFERENCES

[1] *F. Käppeler et al.* The s-process: Nuclear Physics, Stellar Models, Observations. Rev. Mod. Phys., **83** no. 1 (2011) pp. 157–193.

[2] *M. Arnould et al.* The r-process of stellar nucleosynthesis: Astrophysics and nuclear physics achievements and mysteries. *Phys. Rep*, **450** no. 4–6 (2007) pp. 97–213.

[3] *A. Spyrou et al.* Neutron-capture rates for explosive nucleosynthesis: the case of ^{68}Ni(n,γ)^{69}Ni. J. Phys. G: Nucl. Part. Phys., **44** no. 4 (2017) 044002.

[4] *S. Goriely et al.* Comprehensive test of nuclear level density models. Phys. Rev. C, **106** no. 4 (2022) 044315.

[5] *H. Utsunomiya et al.* Photonuclear reaction studies at synchrotron radiation facilities in Japan. Nucl. Phys. A, **738** (2004) 136-142.

[6] *C. Forssen et al.* Determining neutron capture cross sections via the surrogate reaction technique. Phys. Rev. C, **75** no. 5 (2007) 055807.

[7] *M. Guttormsen et al.* The first generation of γ-rays from hot nuclei. Nucl. Instrum. Methods Phys. Res. Section A: Accelerators, Spectrometers, Detectors, and Associated Equipment, **255** no. 3 (1987) 518-523.

[8] *S. N. Liddick et al.* Benchmarking the extraction of statistical neutron capture cross sections on short-lived nuclei for applications using the β-Oslo method. Phys. Rev. C, **100** no. 2 (2019) 024624.

[9] *V. W. Ingeberg et al.* Nuclear level density and γ-ray strength function of ^{67}Ni and the impact on the i-process. *arXiv*.

[10] *S. N. Liddick et. al.* Experimental neutron capture rate constraint far from stability. Phys. Rev. Lett., **116** no. 24 (2016) 242502.

[11] *R. Lewis et. al.* Experimental constraints on the ^{73}Zn (n,γ)^{74}Zn reaction rate. Phys. Rev. C, **99** no. 3 (2019) 034601.

[12] *A. Spyrou et al.* Novel technique for constraining r-process (n,γ) reaction rates. Phys. Rev. Lett., **113** no. 23 (2014) 232502.

[13] *D. Mücher et al.* Extracting model-independent nuclear level densities away from stability. Phys. Rev. C, **107** no. 1 (2022) L011602.

[14] *R. Lewis et al.* Indirect measurement of the (n,γ)^{127}Sb cross section. Phys. Rev. C, **106** no. 1 (2022) 015804.

[15] *D. Rochman et al.* Radiative neutron capture: Hauser Feshbach vs. statistical resonances. Phys. Lett. B, **764** (2017) pp. 109-113 .

[16] *B. Wang et al.* Systematic study of the radiative proton capture including the compound, pre-equilibrium, and direct mechanisms. Phys. Rev. C, **109** no. 1 (2024) 014611.

[17] *C. Iliadis. "Nuclear Physics of Stars"*. Wiley-VCH., (2007).

[18] *T. Raucher*. Sensitivity of astrophysical reaction rates to nuclear uncertainties. ApJS, **201** no. 2 (2012) pp. 26.

[19] *A. Koning et al.* TALYS-1.96/2.0, Simulation of nuclear reactions. (2021).

[20] *S. Goriely et al.* Reference database for photon strength functions. Eur. Phys. J. A, **55** no. 10 (2019).

[21] *Y. Xu et al.* Systematical studies of the E1 photon strength functions combining Skyrme-HFB+QRPA model and experimental giant dipole resonance properties. Phys. Rev. C, **104** no. 4 (2021) 044301.

[22] *Z. Y. Bao et al.* Neutron cross-sections for nucleosynthesis studies. At. Data Nucl. Data Table, **76** no. 1 (2000) pp. 70-154.

[23] https://exp-astro.de/kadonis1.0/.